Similarity of dissociation-recombination phenomena in laminar hypersonic boundary layers

By D. Passiatore AND M. Di Renzo†

1. Introduction

High-speed flows, encompassing objects entering a planetary atmosphere or engaged in atmospheric hypersonic flight, pose a challenging topic of interest for manifold configurations. In the case of such vehicles, the bow shock wave ahead of the body transforms kinetic energy into thermal and chemical energy, potentially dissociating nitrogen and oxygen molecules (Anderson 2019; Bertin & Cummings 2006; Candler 2019; Urzay & Di Renzo 2021). Heat transfer mechanisms in the boundary layer might differ substantially from conventional fluid mechanics, requiring examination of limiting cases to understand various physical processes and compare with experiments. Understanding the intricate dynamics of boundary layers is paramount for the design and performance optimization of high-speed aircraft and spacecraft. The complexity of experimentally studying these phenomena makes numerical simulations of high-speed flows a crucial, albeit complicated, part of this endeavor. From a modeling standpoint, our existing knowledge on cryogenic boundary layers must be extended to chemically reacting flows.
Initially, laminar or transitional flows have started to gain renewed attention (Marxen *et al.* 2014; Mortensen 2015; Kline *et al.* 2019), whereas hypersonic turbulent boundary layers databases have been investigated only recently (Di Renzo & Urzay 2021; Passiatore *et al.* 2021, 2022; Li *et al.* 2022), but the amount of data remains insufficient to draw some general conclusions on universal behavior. Therefore, in view of new works to come, it is important to have a good mastery of some fundamental aspects, such as similarity and its meaning for chemically reacting boundary layers. Self-similar solutions, where the flow characteristics remain invariant under certain scaling transformations, provide invaluable insights into the fundamental nature of hypersonic boundary-layer phenomena. When it comes to chemically reacting flows, the introduction of additional characteristic timescales due to chemistry forces the solution to be only locally self-similar (Liñán & Riva 1962). This change in the nature of the similarity solutions holds profound importance, and its understanding could pave the way toward a thorough description of the dynamics of hypersonic reacting boundary layers in laminar and turbulent conditions.

In this study, we delve into the exploration of locally self-similar conservation equations for a zero-pressure gradient laminar boundary layer with chemical reactions. Solutions of similarity equations have proved to be of utmost importance, starting from inert laminar compressible boundary layers (Fay & Riddell 1958). The original formulation for hypersonic chemically reacting boundary layers is presented in Liñán & Riva (1962) and then specialized for a five-species neutral air mixture with differential diffusion in Di Renzo & Urzay (2021). The current study explores a simplified dissociation-recombination mechanism in an artificial two-species gas mixture. The focus lies on modifying reaction rates to control dissociation levels and examine highly reactive configurations. Therefore, the

† University of Salento, Italy & CTR

novelty of this work with respect to the state of the art consists of a parametric analysis of thermophysical characteristics. In real flight applications, different levels of chemical intensity can occur, depending on the altitude or distance from the leading edge. In order to capture all this variability, one may decide to numerically vary edge and boundary conditions to trigger different scenarios. To simplify the problem, the edge and boundary conditions are fixed, whereas thermophysical parameters are systematically varied. This approach enables a detailed analysis of the interaction between chemistry and diffusive phenomena, exploring chemical similarity.

The remainder of the work is organized as follows. Section 2 reports the similarity conservation equations, as well as the formulation of the chemical mechanism used. In Section 3, the results of the previous set of equations are discussed for different levels of chemical intensity, and the influence of the Reynolds number is also assessed. Finally, Section 4 provides a conclusion and some reflections on future work that may be inspired by this study.

2. Formulation

2.1. *Transport equations*

The two-dimensional boundary-layer conservation equations can be written as

$$\begin{gathered}
\frac{\partial}{\partial x}(\rho u)+\frac{\partial}{\partial y}(\rho v)=0,\\
\rho u\frac{\partial u}{\partial x}+\rho v\frac{\partial u}{\partial y}=-\frac{dP_e}{dx}+\frac{\partial}{\partial y}\left(\mu\frac{\partial u}{\partial y}\right),\\
\rho u\frac{\partial Y_i}{\partial x}+\rho v\frac{\partial Y_i}{\partial y}=-\frac{\partial}{\partial y}\left(\rho Y_i V_{yi}\right)+\dot{\omega}_i,\quad \text{and}\\
\rho u\frac{\partial h_0}{\partial x}+\rho v\frac{\partial h_0}{\partial y}=\frac{\partial}{\partial y}\left(\mu\frac{\partial u}{\partial y}+\lambda\frac{\partial T}{\partial y}-\sum_{i=1}^{N_s}\rho Y_i V_{yi}h_i\right),
\end{gathered}\tag{2.1}$$

where

$$V_{yi}=-\frac{D_i}{X_i}\frac{\partial X_i}{\partial y}+\sum_{i=1}^{N_s}Y_i\frac{D_i}{X_i}\frac{\partial X_i}{\partial y}$$

is the wall-normal component of the diffusion velocity of species. To close the system, the edge pressure P_e is related to the local density and species concentration by the equation of state

$$P_e=\rho R_0 T/\mathcal{M},$$

where the R_0 is the universal gas constant and $\mathcal{M}$ is the mixture molecular weight. Away from the wall in the inviscid shock layer, the boundary layer is subjected to the edge variables

$$\rho=\rho_e,\quad u=U_e,\quad Y_i=Y_{i,e},\quad T=T_e,$$

whereas at the wall

$$u=v=0,\quad \partial Y_i/\partial y=0\quad\text{and}\quad T=T_w.$$

Considering the similarity variables (Lees 1956)

$$\xi(x)=\rho_e\mu_e U_e x\quad\text{and}\quad\eta(x,y)=\frac{U_e}{\sqrt{2\xi}}\int_0^y\rho dy,$$

one can rearrange Eq. (2.1) and obtain their formulation in the self-similar coordinate system

$$(Cf'')' + ff'' = 0, \tag{2.2}$$

$$\left[\frac{C_i Y_i}{Sc_{i,e}}\left(\frac{X_i'}{X_i} - \sum_{j=1}^{N_s}\frac{D_j Y_j}{D_i X_j}X_j'\right)\right]' + fY_i' + 2Da_{c,i}\dot{\mathcal{W}}_i = 0, \quad \text{and} \tag{2.3}$$

$$\frac{c_{p,e}T_e}{h_{0,e}}\left(\frac{C\theta'}{Pr_e}\right)' + fm' + \frac{U_e^2}{h_{0,e}}(Cf'f'')' + \sum_{i=1}^{N_s}\frac{h_{i,e}}{h_{0,e}}\left[\frac{C_i g_i Y_i}{Sc_{i,e}}\left(\frac{X_i'}{X_i} - \sum_{k=1}^{N_s}\frac{D_j Y_j}{D_i X_j}X_j'\right)\right]' = 0, \tag{2.4}$$

where primes denote derivatives with respect to η. Here, $f' = u/U_e$ and $\theta = T/T_e$ are the self-similar parameters for velocity and temperature, respectively. In the previous equations, $C = \rho\mu/\rho_e\mu_e$ is the Chapman-Rubesin parameter and

$$m = \left(\frac{U_e^2}{2h_{0,e}}\right)f'^2 + \sum_{i=1}^{N_s}\left(\frac{h_{i,e}}{h_{0,e}}\right)Y_i g_i, \quad \text{with} \quad g_i = g_{i,ref} + \frac{c_{p,e}^{tr}T_e}{h_{i,e}}\int_{\theta_{ref}}^{\theta}\frac{c_{p,i}^{tr}(\theta)}{c_{p,e}^{tr}}d\theta.$$

In Eqs. (2.3) and (2.4), $C_i = \rho^2 D_i/\left(\rho_e^2 D_{i,e}\right)$ is a dimensionless group of variables similar to the Chapman-Rubesin parameter but for species transport, and $Sc_{i,e} = \mu_e/\left(\rho_e D_{i,e}\right)$ is a Schmidt number based on the edge diffusion coefficient $D_{i,e}$. In Eq. (2.3), $Da_{c,i} = x/\left(U_e t_{c,i}\right)$ is a chemical Damköhler number defined as the ratio of the residence time x/U_e to the characteristic chemical time $t_{c,i}$ based on the edge temperature T_e, with $t_{c,i}$ also used for normalization of the chemical production rate as $\dot{\mathcal{W}}_i = t_{ch,i}\dot{w}_i/\rho$. For the sake of clarity, in the case of frozen chemistry or chemical equilibrium, the only ξ-dependent term in Eq. (2.3) vanishes and the resulting equations become globally self-similar.

The previous system of equations can be integrated numerically, subject to boundary conditions

$$\begin{array}{llll} f' = f = 0, & Y_n' = 0, & \theta = \theta_w & \text{for} \quad \eta = 0, \quad \text{and} \\ f' = 1, & Y_n = Y_{n,e}, & \theta = 1 & \text{for} \quad \eta \to \infty. \end{array}$$

2.2. *Thermochemical models*

In order to simplify the problem and isolate the effects of the chemical mechanism, we are considering an artificial two-species mixture composed of two species, M_2 and M. It can be envisioned as any two-species mixture (e.g., molecular oxygen/atomic oxygen), subject to the simple dissociation-recombination mechanism

$$\mathrm{M_2} \Longleftrightarrow 2\mathrm{M}.$$

Specific heats and enthalpies are evaluated using the nine-coefficient NASA polynomials (McBride *et al.* 2002) particularized for molecular and atomic oxygen. Sutherland's law is used to compute viscosity, while the thermal conductivity of the mixture is computed with the constant Prandtl number assumption $\mathrm{Pr} = c_p\mu/\lambda = 0.71$. To conclude, a constant Schmidt number $Sc_i = \mu/\left(\rho D_i\right) = 0.5$ is utilized for both species to obtain mass diffusion coefficients. The previous approximations may be inappropriate for high-temperature chemically reacting gases; nevertheless, the goal of the present work is to assess dissociation-recombination mechanism behavior uniquely; therefore the previous

M_e	Re_{δ^*}	T_e [K]	T_w/T_e	$c_{p,e}T_e/h_{0,e}$	$U_e^2/h_{0,e}$
10	15000	500	5	0.05	1.96

TABLE 1. Edge and dimensionless parameters of the present test case.

modeling choices are made to isolate the nonequilibrium chemistry effects in this theoretical study. The chemical source term of M_2 is computed following the law of mass action

$$\dot{\omega}_{M_2} = k_f \left(\frac{\rho Y_{M_2}}{\mathcal{M}_{M_2}} \right) - k_b \left(\frac{\rho Y_M}{\mathcal{M}_M} \right)^2, \tag{2.5}$$

where $\mathcal{M}_\bullet$ is the species' molecular weight. In Eq. (2.5), k_f is the forward reaction rate, computed as

$$k_f = A T^n \exp\left(\frac{-E_a}{R_0 T} \right), \tag{2.6}$$

whereas $k_b = k_f / K_{\text{eq}}$ is the backward reaction rate, with K_{eq} being the equilibrium constant, as a function of Gibbs free energy. Being K_{eq} unequivocally defined by the thermodynamic state of the mixture, one can only manipulate the terms A and E_a in Eq. (2.6), corresponding to the pre-exponential factor and activation energy of a reaction, respectively, to trigger different scenarios. In the following, the temperature exponent n is fixed and equal to -1.5. To have an idea of the order of magnitude of these parameters in a five-species air mixture, the reaction corresponding to the dissociation of molecular oxygen is characterized by $A = 2 \times 10^{15}$ m^3/(mol s) and $E_a/R_0 = 59\,500$ K, in contrast to the dissociation of nitrogen, which has $A = 7 \times 10^{15}$ m^3/(mol s) and $E_a/R_0 = 113\,200$ K. As a result, dissociation of molecular oxygen starts already at $T = 2550$ K, whereas molecular nitrogen starts to dissociate at $T = 4000$ K. Having these orders of magnitudes in mind, the remainder of the paper will present results in which these parameters are varied in order to trigger a specific amount of dissociation at moderate freestream conditions.

3. Discussion

The main thermofluid dynamic parameters that define the analyzed cases are listed in Table 1. The different solutions are obtained by keeping these parameters fixed. Note that, the Re_{δ^*} corresponds to different Re_x when the chemistry mechanism is varied. We now consider the dissociation-recombination mechanisms defined in Table 2.

The pre-exponential factors of the four cases in Table 2 are fixed, whereas activation energy is changed. Figure 1 shows the similarity solution profiles for the four test cases, plotted against the similarity variable. The trend of the velocity profiles, shown in Figure 1(a), clearly demonstrates that, despite the different chemical activity in the mixture, the dynamic field is not affected by the amount of atomic species, the momentum equation being somehow weakly coupled with the species composition via density changes. This result has already been observed in numerical simulations of turbulent boundary layers (Di Renzo & Urzay 2021; Passiatore *et al.* 2021), where the existing scaling and correlations, such as incompressible velocity transformations, were proved to be still valid in the presence of chemical reactions. In contrast, the profiles of temperature in figure 1(b) are

Legend	Label	A [m^3/(mol s)]	E_a/R_0 [K]	Da_1	Da_2	Da_3
———	BL1	10^{15}	40×10^3	1.847×10^{-4}	2.083×10^{-3}	4.454×10^{-5}
- - - -	BL2	10^{15}	45×10^3	1.778×10^{-4}	6.068×10^{-4}	8.631×10^{-5}
———	BL3	10^{15}	50×10^3	1.341×10^{-4}	1.352×10^{-4}	9.246×10^{-5}
- - - -	BL4	10^{15}	60×10^3	2.771×10^{-5}	2.771×10^{-5}	2.055×10^{-5}

TABLE 2. Parameters for the four chemical mechanisms analyzed. Of note, Da_1, Da_2 and Da_3 will be defined afterwards in Eqs. (3.3)–(3.5), respectively.

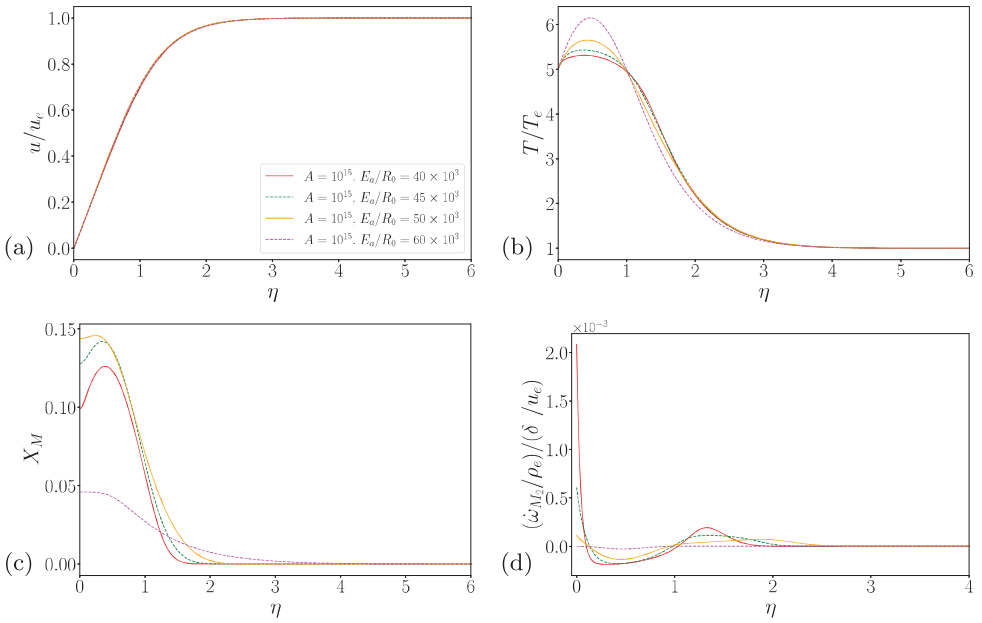

FIGURE 1. (a) Similarity velocity profile, (b) temperature profile, (c) molar fraction of atomic species and (d) chemical source term of molecular species (d), for the four test cases.

strongly influenced by the intensity of the chemical source terms. Dissociation reactions are endothermic in the forward direction, draining energy from the boundary layer and resulting in higher temperatures when chemical activity is lower. All the profiles exhibit a nonmonotonic behavior due to wall cooling, but as the activation energy decreases, the profiles are flatter and have lower temperature peaks. From this point of view, the temperature plots are closely related to the dissociation activation energies (i.e., BL1 exhibits the lowest temperature peak).

As for the evolution of the species molar fractions, some observations are in order. First of all, with these values of activation energy, we have spanned a concentration range of dissociated species that goes from 4.5% up to 14%. Note that boundary-layer results present in literature (so far) exhibit dissociation of molecular oxygen up to one-third of the total amount, meaning that the values proposed in this work are consistent with the full air mechanism and can give us confidence in this simplified mixture. The most important finding when going to such high chemical intensity is the nonmonotonicity of the profiles according to the levels of activation energy. Indeed, one would expect the same

considerations of temperature profiles: The peak of dissociation increases with decreasing activation energy. In fact, when the activation energy of the dissociation reaction is low, the k_f of the reaction is overall higher in the entire boundary layer. Instead, even though the smallest amount of atomic species corresponds to the highest activation energy in case BL4, as expected, comparing BL1, BL2 and BL3, the maximum concentration of X_M is observed for BL3 and the lowest for BL1. This trend is due mainly to the two competing mechanisms of diffusion and chemistry.

The equilibrium constant of the considered chemical reaction, which is determined by minimizing the total free energy of the system, is only a function of the temperature, as previously said. Thus, the ratio between k_f and k_b is similar among all the test cases considered in this study. Since the wall temperature is sufficiently low to induce an equilibrium constant of the chemical reaction that is biased toward the nondissociated side, the near-wall recombination rate becomes increasingly more intense as E_a decreases. This is confirmed by the trend of the normalized chemical source terms, shown in Figure 1(d). By looking at the profile for BL1, one can see that $\dot{\omega}_{M_2}$ exhibits the highest value among all the four test cases at the wall. This value being positive, recombination reactions are active, explaining why such a low value of X_M is present at the wall with respect to the cases with higher activation energy. The high amount of X_M for BL3 at the wall is then justified by diffusion phenomena. Therefore, significant dissociation has taken place further away from the wall, and the dissociation products have been transported to the wall by diffusion at a rate that is much higher than recombination. In the BL1 case, the chemical dissociation happens again away from the wall but, as the diffusion brings the atomic M close to the wall, the recombination is able to transform a significant portion of dissociated species back into molecular form. Case BL2 is somewhere in the middle between the two extremes just explained.

3.1. *Damköhler number*

The competition between diffusion and chemical activity makes the definition of an appropriate Damköhler number of fundamental importance. In Section 2, we defined a Damköhler number as a ratio between the flow residence time and a characteristic chemical timescale

$$Da_{c,i} = x/\left(U_e t_{c,i}\right). \tag{3.1}$$

While the definition of the flow timescale is straightforward in this framework, the chemical timescale, called here after t_c and being equal with opposite sign for the two species of this mixture, is not trivial. Given that the following study is performed at a fixed Reynolds number based on the displacement thickness and, as already anticipated, the computed streamwise station x is different for the four test cases, we prefer to use a flow timescale based on δ^*

$$Da = \delta^*/\left(U_e t_c\right). \tag{3.2}$$

For the sake of clarity, this choice is completely arbitrary, and the previous study may have been performed at the same Re_x, resulting in the choice of the flow residence time as the most reasonable option. The numerator of Da being fixed, a global definition of the chemical timescale should be adopted as well. The chemical timescale is generally computed as $\rho/\dot{w}_i$, but what specific values of both the source terms and the density

should be used is here under investigation. The options being considered are

$$Da_1 = \delta^*/(U_e t_{c,1}), \qquad t_{c,1} = \frac{\rho_e}{\dot{\omega}_{|\mathrm{Tmax}}}, \tag{3.3}$$

$$Da_2 = \delta^*/(U_e t_{c,2}), \qquad t_{c,2} = \frac{\rho_e}{|\,\dot{\omega}_{\max}\,|}, \quad \text{and} \tag{3.4}$$

$$Da_3 = \delta^*/(U_e t_{c,3}), \qquad t_{c,3} = \left(\frac{1}{\delta_c}\int_0^{\delta_c} (\dot{\omega}/\rho)\right)^{-1}. \tag{3.5}$$

In Eq. (3.3), the source term corresponding to the maximum temperature is used. Another definition in Eq. (3.4) consists of taking the maximum value of the source term. In the previous formulations, Eq. (3.4) has been used by Di Renzo & Urzay (2021), whereas the introduction of Eq. (3.3) is useful to characterize the cases in which the production rate does not match with the trend of temperature due to diffusion phenomena. Lastly, the integral of the reaction rate from zero to a certain chemical characteristic thickness δ_c is considered; the latter has been computed as the farthest point from the wall at which the molar fraction is equal to 1% of the maximum X_M value, i.e., $\delta_c = 0.01 X_{M_{|\max}}$. The choice of considering a chemical thickness rather than the boundary-layer thickness is due to the dynamic/chemistry weak coupling. For the considered test cases, the boundary-layer thickness δ, computed as 99% of the edge velocity, is approximately the same for all cases and corresponds to $\eta \approx 2.5$. When computing δ_c instead, it is possible to capture the variability of the dissociating layers. As a result, this thickness is equal to 1.56, 1.75, 2.06 and 3.78, from BL1 to BL4, respectively. The possibility of introducing an integral scale relies on the coexistence of dissociation and recombination, i.e., negative and positive values of $\dot{\omega}_{M_2}$; performing the integral of the source term is a smart way to take into account both production and depletion.

In the attempt to find the dimensionless parameter that reflects the order of maximum dissociation, we have computed all the definitions of the previous chemical timescales to compute the Damköhler numbers for all test cases. Those values are reported in Table 2. The order of the Damköhler numbers for the definitions in Eqs. (3.3) and (3.4) strictly follows the order of the activation energy, the highest Damköhler number corresponding to the lowest activation energy. Besides, for the case BL4, Da_1 and Da_2 are basically identical, proving that the chemical source terms tightly follow the trend of the temperature at such low chemical intensity. The definition of Da_3 appears to be the most appropriate to represent the chemical dissociation level in the boundary layer. Indeed, the highest Damköhler number is the one with the maximum concentration of X_M in the boundary layer, corresponding to BL3; in order, test case BL2 has a slightly smaller value, followed by BL1. Lastly, the case with the highest activation energy exhibits the lowest value.

Another way to investigate similarity is to verify that a different combination of physical parameters may lead to a self-similar solution. As a confirmation, we have selected another case in which both the pre-exponential and the activation energy are varied, namely: $A = 7 \times 10^{15}$ [m^3/(mol s)], $E_a/R_0 = 45\,000$ K with $Da_3 = 3 = 4.625 \times 10^{-5}$, in order to have a similar trend to the test case BL1. Figure 2 shows the evolution of temperature and molar fraction profiles for the new case and BL1. Given that the profiles almost perfectly superpose, one can say that the similarity is preserved, even with a different combination of physical parameters, if the dimensionless numbers defined are the same. As a matter of fact, this new test case presents $Da_1 = 1.846 \times 10^{-4}$, $Da_2 = 1.989 \times 10^{-3}$

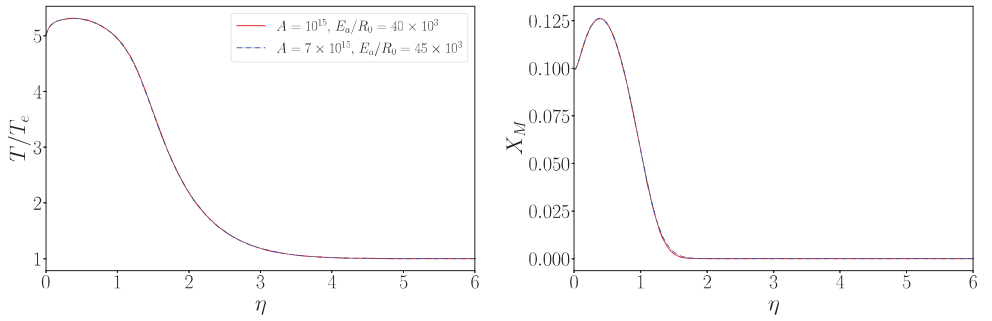

FIGURE 2. Similarity solution of species molar fractions for two cases with similar Damköhler number: BL1 (red curve) and $A = 7 \times 10^{15}$ [m^3/(mol s)], $E_a/R_0 = 45000$ K (blue curve).

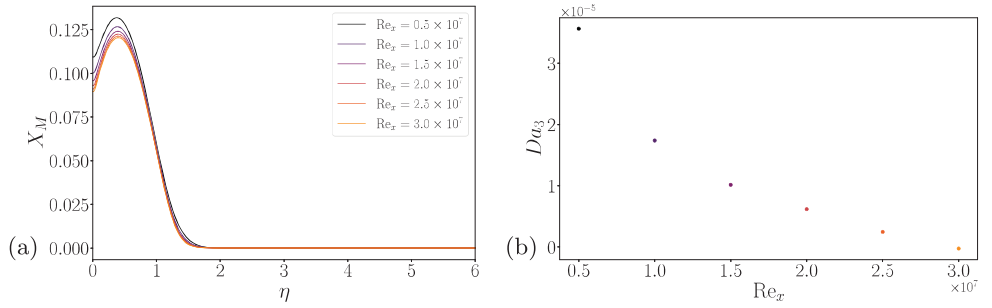

FIGURE 3. (a) Similarity solution of X_M and (b) streamwise evolution of Da_3 (b), for case BL2.

and $Da_3 = 3 = 4.625 \times 10^{-5}$, which are almost identical to the dimensionless numbers of case BL1.

3.2. *Effect of Reynolds number*

The results analyzed so far are extracted at a fixed Reynolds number based on the displacement thickness, though the corresponding Re_x is slightly different. In this section, we analyze the trend of the molar fractions at different Re_x values. We consider case BL2, which exhibits the nonmonotonic trend of the species molar fractions. Results are shown in Figure 3(a). When the diffusion terms are smaller than the chemical terms and the recombination reactions play an important role, as for the case BL2, the effect of the Reynolds number results in decreasing the maximum amount of atomic species. Also, the relative difference in concentration between different Re_x values become smaller and smaller. In Figure 3(b), we also plot the streamwise evolution of Da_3. According to the evolution of the peak of X_M, Da_3 is getting smaller, meaning that the chemical timescales are becoming larger; also, the mild variations in chemical concentration after $Re_x = 2.0 \times 10^7$ mean that BL2 is going toward a quasi-frozen chemical state, justified by the increasing chemical timescales.

3.3. *Solution of air mixture*

For the sake of completeness, we have computed the similarity solution for the air mixture composed of N_2, O_2, NO, O and N. The conditions of this test case are $Re^*_\delta = 5000$, $T_e = 1000$ K, $T_w/T_e = 1.5$ and $M_e = 9.85$. The aim of this section is to prove that the previous analyses can be easily extended to a nonbinary mixture that is more representative of

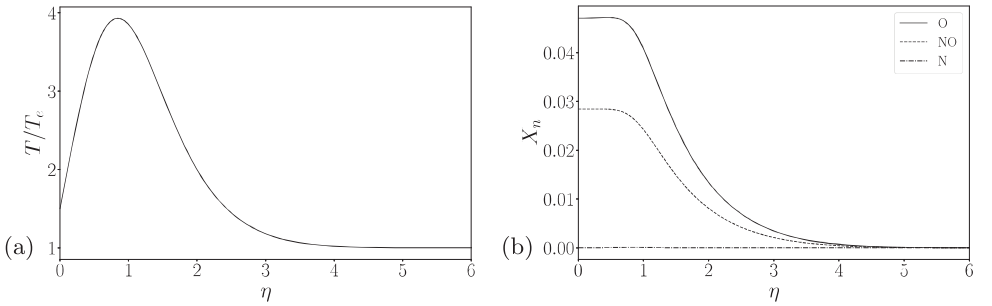

FIGURE 4. Evolution of (a) the temperature profile and (b) molar fractions profiles (b) for the similarity solution of air mixture.

practical configurations. The results are shown in Figure 4. Focusing uniquely on atomic oxygen, the present configuration results in a monotonic trend of species molar fractions, meaning that the diffusion phenomena are dominant in the near-wall region, at least at this Reynolds number. Additionally, the maximum molar fraction of atomic species reached is approximately 4.5%, similar to BL4 in the previous case. As a confirmation, the dimensionless number computed in this case for the atomic oxygen is $Da_{3,O} = 2.106 \times 10^{-5}$, similar to the Da_3 of case BL4, as expected. Therefore, even when using a nonbinary mixture, the definition of this Damköhler number can already give an idea of rate of the reactions. Ongoing efforts are dedicated to finding an *a-priori* estimation of δ_c and, consequently, of Da_3, so that one can already select the test case targeting a specific amount of dissociated species.

4. Conclusions

The exploration of locally self-similar conservation equations for the laminar boundary layer with chemical reactions represents a significant stride in comprehending the intricate dynamics of hypersonic flows. Through our study, we have probed some fundamental aspects of hypersonic high-temperature boundary layers, shedding light on the budget between chemistry and diffusive phenomena. By delving into a simplified dissociation-recombination mechanism, we have shown that when the activation energy is small enough to trigger strong chemical activity, the profile of the molar fractions faithfully follows the profile of the temperature. Consequently, the maximum percentage of dissociation decreases, contrary to what is expected, and the dissociation peak corresponds to the temperature peak. In this situation, an increase in Reynolds number would augment this effect, further decreasing the peak of atomic species and eventually leading to a quasi-frozen chemistry. When the activation energy is higher (yet still low enough to have significant chemical activity), diffusion phenomena play the most important role and the profiles of the species molar fractions are monotonic. The maximum concentration of atomic species is found at the wall, with products being transported by diffusion. In the attempt to categorize the diffusion/chemistry interplay, different Damköhler numbers have been considered. The most appropriate choice considers a chemical timescale based on the integral of the reaction rate from the wall up to the thickness of the dissociating layer. This dimensionless number is able to respect the order of maximum dissociation rather than the order of the imposed activation energy, the two aspects not being necessarily aligned.

This study is a preliminary work to understand the similarity of chemistry in laminar hypersonic boundary layers. An analogous study can be extended to the interaction between wall-normal turbulent mixing and chemical dissociation/recombination processes. This investigation will eventually aim to determine whether turbulent correlations or scaling for species' average and fluctuating quantities can be identified, similar to how we analyze other thermodynamic properties.

Acknowledgments

This investigation was funded by the Advanced Simulation and Computing program of the U.S. Department of Energy's National Nuclear Security Administration via the PSAAP-III Center at Stanford, Grant No. DE-NA0003968.

REFERENCES

Anderson, J. D. 2019 *Hypersonic and High-Temeprature gas dynamics*, 3^{rd} ed. American Institute of Aeronautics and Astronautics.

Bertin, J. J. & Cummings, R. M. 2006 Critical hypersonic aerothermodynamic phenomena. *Annu. Rev. Fluid Mech.* **38**, 129–157.

Candler, G. 2019 Rate effects in hypersonic flows. *Annu. Rev. Fluid Mech.* **51**, 379–402.

Di Renzo, M. & Urzay, J. 2021 Direct numerical simulation of a hypersonic transitional boundary layer at suborbital enthalpies. *J. Fluid Mech.* **912**, A29.

Fay, J. A. & Riddell, F, R. 1958 Theory of stagnation point heat transfer in dissociated air. *J. Aeronaut. Sci.* **25**, 74–85.

Kline, H. L., Chang, C. & Li, F. 2019 Multiple boundary layer instability modes with nonequilibrium and wall temperature effects using LASTRAC. In *AIAA Aviation 2019 Forum*, p. 2850.

Lees, L. 1956 Laminar heat transfer over blunt-nosed bodies at hypersonic flight speeds. *J. Jet Propulsion* **26**, 259–269.

Li, J., Yu, M., Sun, D., Liu, P. & Yuan, X. 2022 Wall heat transfer in high-enthalpy hypersonic turbulent boundary layers. *Phys. of Fluids* **34** (8).

Liñán, A. & Riva, I. D. 1962 Chemical nonequilibrium effects in hypersonic aerodynamics. In *Third Int. ICAS Congr.* Stockholm: International Council of the Aeronatuical Sciences.

Marxen, O., Iaccarino, G. & Magin, T. E. 2014 Direct numerical simulations of hypersonic boundary-layer transition with finite-rate chemistry. *J. Fluid Mech.* **755**, 35–49.

McBride, B. J., Zehe, M. J. & Gordon, S. 2002 NASA Glenn coefficients for calculating thermodynamic properties of individual species. *Tech. Rep.* NASA/TP-2002-211556.

Mortensen, C. H. 2015 Effects of thermochemical nonequilibrium on hypersonic boundary-layer instability in the presence of surface ablation or isolated two-dimensional roughness. PhD thesis, UCLA.

Passiatore, D., Sciacovelli, L., Cinnella, P. & Pascazio, G. 2021 Finite-rate chemistry effects in turbulent hypersonic boundary layers: A direct numerical simulation study. *Phys. Rev. Fluids* **6**, 054604.

Passiatore, D., Sciacovelli, L., Cinnella, P. & Pascazio, G. 2022 Thermochem-

ical non-equilibrium effects in turbulent hypersonic boundary layers. *J. Fluid Mech.* **941**, A21.

Urzay, J. & Di Renzo, M. 2021 Engineering aspects of hypersonic turbulent flows at suborbital enthalpies. *Annual Research Briefs,* Center for Turbulence Research, Stanford University, pp. 7–32.